Aerosol optical properties over east Asia determined from ground-based sky radiation measurements

Do-Hyeong Kim,[1] Byung-Ju Sohn,[1] Teruyuki Nakajima,[2] Tamio Takamura,[3] Toshihiko Takemura,[4] Byoung-Cheol Choi,[5] and Soon-Chang Yoon[1]

Received 8 January 2003; revised 21 March 2003; accepted 2 June 2003; published 29 January 2004.

[1] Aerosol optical properties (aerosol optical thickness, Ångström exponent, size distribution, and single scattering albedo) over east Asia were examined using long-term measurements of sky radiation at Mandalgovi, Dunhuang, Yinchuan, and Sri-Samrong sites of the Skyradiometer Network (SKYNET). Also included were sky radiation measurements at Anmyon, Gosan in Korea, and Amami-Oshima in Japan during April for examining optical properties of Asian dust. Results show that the seasonal average of aerosol optical thickness (AOT) generally exhibits a maximum in spring and a minimum in autumn over east Asia. At Sri-Samrong and Yinchuan, relatively distinct seasonal cycles are noted, in comparison to the arid desert regions of Dunhuang and Mandalgovi. In general, aerosol size distributions are characterized by a bimodal pattern, with a fine mode around 0.2 μm and a coarse mode around 2−5 μm. Similar to AOT and α, volume spectra are also much dependent on geographical location and season. Dunhuang mostly shows coarse mode particles in all seasons, while Mandalgovi and Sri-Samrong show large seasonal variations in the total volume of fine mode particles. The single scattering albedos of dust particles over east Asia are around 0.9 at 0.5 μm, which are larger than the previously known values of 0.63–0.89 but similar to those found in the Aerosol Robotic Network (AERONET) analysis. It is noted that the optical properties of Asian dust around Korea and Japan are quite similar to those found in dust source regions such as Dunhuang and Mandalgovi. However, the single scattering albedo appears to be smaller than those observed in Dunhuang and Mandalgovi. Furthermore, single scattering albedo tends to become smaller during the dust outbreak period. Considering that aerosols in Korean and Japanese areas are much influenced by anthropogenic aerosols emitted in China particularly under the westerly conditions, the mixing processes between different aerosol species may be the cause of the different optical properties of Asian dust. *INDEX TERMS:* 0305 Atmospheric Composition and Structure: Aerosols and particles (0345, 4801); 0322 Atmospheric Composition and Structure: Constituent sources and sinks; 3309 Meteorology and Atmospheric Dynamics: Climatology (1620); 3359 Meteorology and Atmospheric Dynamics: Radiative processes; *KEYWORDS:* aerosol optical property, sky radiation measurements, Asian dust

Citation: Kim, D.-H., B.-J.Sohn, T. Nakajima, T. Takamura, T. Takemura, B.-C. Choi, and S.-C. Yoon (2004), Aerosol optical properties over east Asia determined from ground-based sky radiation measurements, *J. Geophys. Res.*, *109*, D02209, doi:10.1029/2003JD003387.

1. Introduction

[2] It is well known that aerosols can have a profound impact on the global and regional climate, both by directly interacting with solar radiation and by indirectly modifying cloud microphysics [e.g., *Russell et al.*, 1999; *Satheesh et al.*, 1999; *Nakajima et al.*, 2001]. The global average of the associated annual radiative forcing by aerosols at the top of the atmosphere (TOA) ranges from 0 to -2 W m^{-2}, which is comparable to the forcing induced by the increase in greenhouse gas concentration during the last century [*Intergovernmental Panel on Climate Change* (*IPCC*), 2001]. However, it is noted that aerosol-induced radiative forcing is subject to an uncertainty of more than a factor of

[1]School of Earth and Environmental Sciences, Seoul National University, Seoul, South Korea.
[2]Center for Climate System Research, University of Tokyo, Tokyo, Japan.
[3]Center for Environmental Remote Sensing, Chiba University, Chiba, Japan.
[4]Research Institute for Applied Mechanics, Kyushu University, Fukuoka, Japan.
[5]Meteorological Research Institute, Korea Meteorological Administration, Seoul, South Korea.

0148-0227/04/2003JD003387$09.00

two [*Haywood and Ramaswamy*, 1998; *Jacobson*, 2001]. Accordingly, *IPCC* [2001] reported that the uncertainties induced by different contributing factors should be resolved in order to estimate the overall uncertainty in the direct/indirect forcing estimates.

[3] Compared to atmospheric gaseous constituents, a great deal of these uncertainties is stemmed from inhomogeneity and variability of aerosols in space and time. There are significant variabilities of the aerosol optical properties because of not only aerosol types but also source characteristics related to different origins. There are also seasonal and interannual variabilities even if a certain aerosol type is prevailing at one location, because of different meteorological characteristics [e.g., *Eck et al.*, 2001; *Dubovik et al.*, 2002a].

[4] Thus it is of interest to examine aerosol characteristics over east Asia where aerosol sources are presumed to be much different from other regions. There are many absorbing soot and organic aerosols from coal or biomass burning over the Asian and Pacific regions [*Chameides et al.*, 1999]. Increased fossil fuel burning caused by rapid economic growth in many Asian countries results in more SO_2, organic matters, and soot aerosols emitted into the east Asian atmosphere. The oxidizing environment of the atmosphere is likely to change as the growing transportation sector raises levels of nitrogen oxides to levels like those in Europe and North America [*van Aardenne et al.*, 1999]. Moreover, Asian dust particles, which could lead to both cooling by scattering sunlight back to space and warming by absorbing solar and infrared radiation, make the Asian aerosol situation more complicated [*Sokolik and Toon*, 1999]. The fact that much of the Asian aerosols blow out over the Pacific under westerlies implies that significant changes in radiative forcing may be expected over large adjacent areas.

[5] Because of the interest in dust impact on the local and global climate, field experiments were conducted over the east Asian seawaters. The Asian-Pacific Regional Aerosol Characterization Experiment (ACE-Asia) was conducted over the East China Sea to determine the physical, chemical, and radiative properties, and to quantify the interactions between aerosols and radiation, and the physical and chemical processes controlling the evolution of the major aerosol types (see http://saga.pmel.noaa.gov/aceasia). In addition, aiming at understanding and modeling the impact of aerosol on radiation budget and precipitation efficiency in conjunction with cloud system over east Asia, the Asian Atmospheric Particle Environmental Change Studies (APEX) are being conducted over the Japanese Amami-Oshima area [*Nakajima et al.*, 2003].

[6] Apart from those experiments over the east Asian seawaters, a ground-based aerosol/radiation observation network named as the Skyradiometer Network (SKYNET) (see http://atmos.cr.chiba-u.ac.jp/aerosol/skynet for details) was established in late 1997 for studying the role of aerosol in climate over the large-scale Asian continent as a part of GEWEX Asian Monsoon Experiment/Asian Automatic Weather Station Network (GAME/AAN). This experiment inherits earlier studies on Sun/sky photometry measurements of aerosol over east Asia, e.g., *Cho* [1981] from 1976 to 1977 in Seoul, Korea; *Shiobara et al.* [1991] from 1981 to 1985 in Sendai, Japan; *Qiu et al.* [1987] in Beijing, China. Multiyear data are now available, from which seasonal and interseasonal variations of aerosol properties on a regional scale can be examined. The SKYNET currently continues to operate instruments including skyradiometer, pyranometer, and pyrheliometer for the long-term monitoring of aerosol influences on the east Asian climate system. In this study, we present analysis results from the SKYNET experiment from 1998 to 2000 to describe long-term characteristics and variations of aerosol optical properties over the east Asian continent. As a part of this research, we also examine sky and solar radiation measurements during the spring of 1998 to 2001 at two Korean sites (Anmyon and Gosan) and one Japanese measurement site (Amami-Oshima), focusing on the examination of optical characteristics of Asian dust.

2. Observations and Analysis

[7] Direct and diffuse solar radiation measurements were carried out using the sky radiometer (POM-01L; Prede Co. Ltd.) at seven wavelengths of 315, 400, 500, 675, 870, 940, and 1020 nm at eight measurement sites given in Figure 1, during the period from 1998 to 2000.

[8] It must be worthwhile describing the geographical and climatological features of the observation sites because they are the main elements determining local aerosol characteristics. Mandalgovi is located at the northern most latitude among the measurement sites. It is located in the arid region at the north of the Gobi desert and surroundings are mainly grasses. Dunhuang is located in the east of the Taklimakan desert, thus dust influences seem to be far more significant. Yinchuan is an urban area that may produce much of organic carbons. At the same time, because Yinchuan is located between the Gobi desert in the north and yellow loess in the southeast, dust particles may be easily transported from surroundings when northerlies or south-easterlies are prevalent. Since regions bounded by (35°N–50°N; 80°E–90°E) and (35°N–50°N; 100°E–110°E) are considered as the source regions for Asian dust, Madalgovi, Dunhuang, and Yinchuan are expected to experience high frequencies of the dust event under the strong wind speed and lower relative humidity conditions during the spring time, while Hefei is in the dust outflow region. Sri-Samrong is located in the tropical zone, but the observation site is surrounded by the crop-testing field which sometimes has no vegetation but bare soil. Thus it is natural to observe dusts locally uplifted during the winter dry season. Located in the Asian monsoon region, Sri-Samrong shows three distinct seasons; winter (mid-October to mid-February), rainy (mid-May to mid-October), and summer or premonsoon season (mid-February to mid-May). In addition, forest fires are frequently observed in this area during the dry winter season.

[9] Detailed observation periods are provided in Figure 2. Beside the above mentioned SKYNET measurements, field experiments for the Asian dust were also carried out at Anmyon during the springtime of 1998–2000, Gosan during April of 2001, and at Amami-Oshima during April of 2001. The periods for acquired data are also given in Figure 2.

[10] The aerosol optical thickness, single-scattering albedo at five wavelengths (400, 500, 675, 870, and 1020 nm), Ångström exponent, and volume size distribution ($dV(r)/d\ln r$ (cm^3cm^{-2})) were retrieved using the SKYRAD.pack software (version 3), developed at The University of Tokyo,

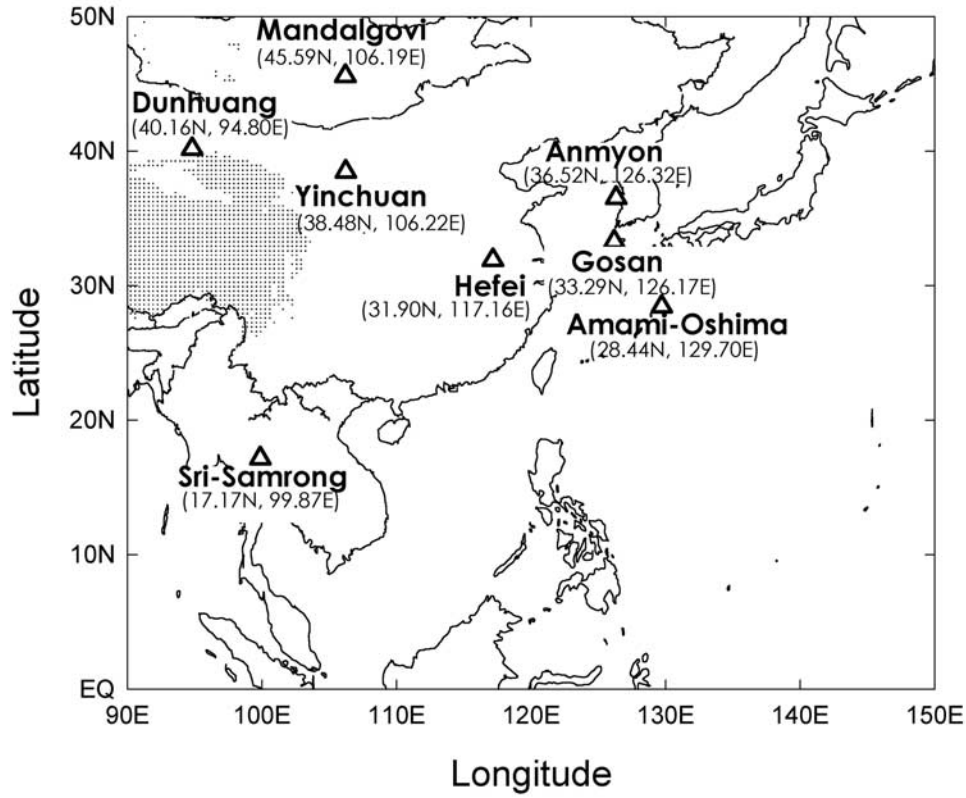

Figure 1. Geographical locations of observation sites.

which consists of a radiative transfer code as well as linear and nonlinear inversion components [*Nakajima et al.*, 1996]. Brief summary of the inversion method is found in Appendix A, along with some results from the sensitivity test for uncertainty analysis.

[11] The algorithm used in this study is based on spherical particle assumption. However, for the accurate retrieval of aerosol properties from sky radiation measurements, it is important to consider the influences of nonspherical particles, especially of desert dust particles because retrieved results seem to show unrealistic spectral dependence in the real part of the refractive index and artificially increased fine particle mode [*Dubovik et al.*, 2000, 2002b]. The retrieved phase function also exhibits significant differences when spherical particles are assumed, but not to a degree to significantly alter single scattering albedo [*Dubovik et al.*, 2000, 2002b]. By contrast, our results do not show such an artificially increased fine mode. Those discrepancies may be due to the independent algorithm for the AERONET or invariant complex refractive index with wavelength in the algorithm used in this study. Nonetheless influences of nonsphericity are better to be included for improving the retrieval qualities for large dust particles.

[12] For the retrieval of aerosol optical properties we first remove cloud-contaminated measurements by using the cloud screening method by *Smirnov et al.* [2000], which uses the difference of AOT between two consecutive measurements as a criterion determining the clear-sky condition. However, instead of using 0.02 of *Smirnov et al.* [2000] determined from Aerosol Robotic Network

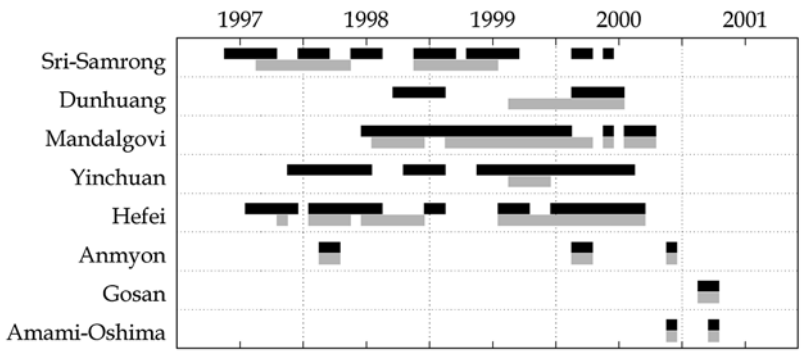

Figure 2. The observation periods covered by five SKYNET measurements sites and at the Anmyon, Gosan, and Amami-Oshima sites. Black and gray-stripe solid lines represent the periods of skyradiometer observations, and pyranometer/pyrheliometer observations, respectively.

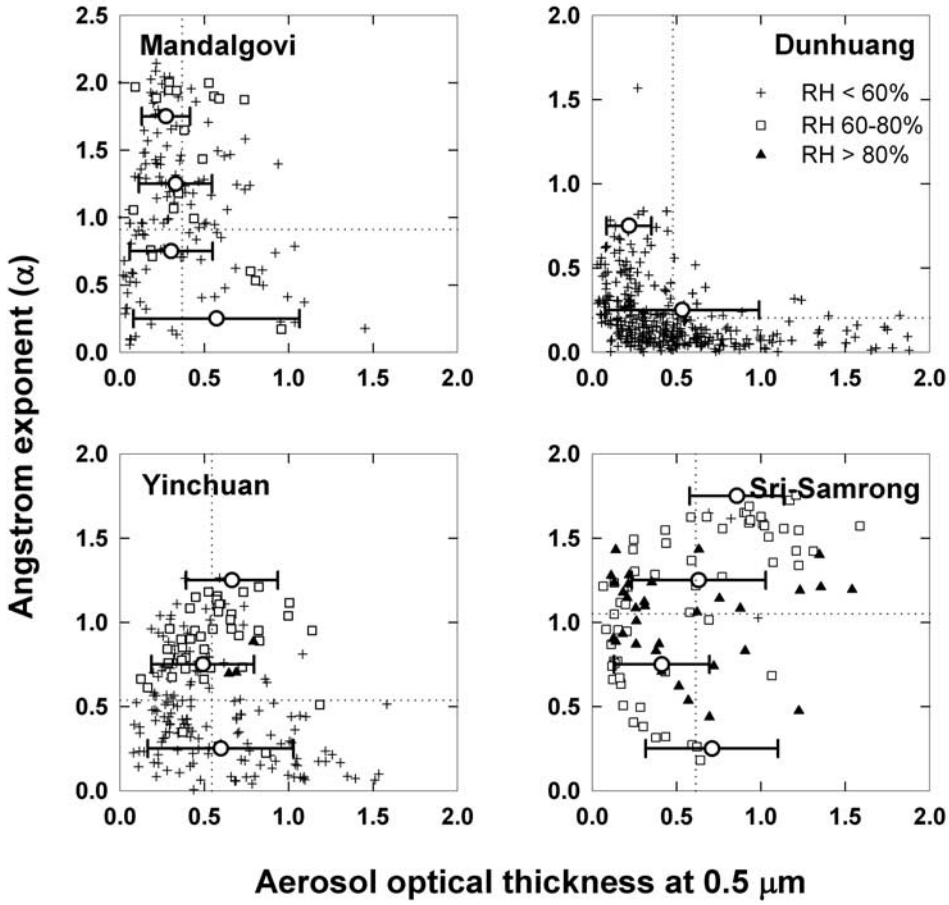

Figure 3. Scatterplots of daily averaged aerosol optical thickness at 0.5 μm (AOT) and Ångström exponent (α) with different relative humidity (RH) range (cross hair, square, and triangle for 0–60%, 60–80%, and 80–100%, respectively). The dotted lines are for mean values of α-AOT. Open circles and error bars indicate AOT averages and the standard deviations given at four α ranges (0–0.5, 0.5–1.0, 1.0–1.5, 1.5–2.0). Symbols for RH are given in the upper right panel.

(AERONET) measurements over the globe, we use the empirically determined value of 0.03 as a threshold value because the aerosol variations tend to be larger over east Asia in particular during the dust season. Even if data pass the threshold screening test, we only take data within three standard deviations from the mean in order to further reduce uncertainties induced by cloud contamination.

[13] The cloud-filtered radiances are inserted into the retrieval algorithm, and then the calculated radiances using the retrieved aerosol parameters are compared against measured values. Retrievals are discarded if the difference between observed and calculated radiance is greater than 7% in an absolute sense.

3. Results

[14] In this section, we present analysis results obtained from sky radiation measurements over east Asia. We first pay attention to the seasonal and interseasonal variations of optical properties shown in the measurements at SKYNET sites, and then the optical properties of Asian dust will be discussed using special measurements at Anmyon, Gosan, and Amami-Oshima.

3.1. Long-Term Characteristics

3.1.1. Aerosol Optical Thickness and Ångström Exponent

[15] Sky radiation measurements taken at Mandalgovi, Dunhuang, Yinchuan, and Sri-Samrong during the period from 1998 to 2000 were used for the retrieval of aerosol optical parameters. In this analysis, measurements at Hefei were not included because there is no information about the solid viewing angle of skyradiometer which should be used as input to the retrieval algorithm. The sensitivity of the retrieved optical thickness to the solid viewing angle suggests that misdiagnosed angle can induce an error up to 30% of the optical thickness, especially under thin optical thickness conditions.

[16] Scatterplots of daily mean AOT at 0.5 μm versus Ångström exponent (α) are given in Figure 3. Mean AOTs for the four α ranges (i.e., 0–0.5, 0.5–1.0, 1.0–1.5, and 1.5–2.0) are given in circles with bars indicating the respective

standard deviation. Ångström exponent (α) is defined by the wavelength dependence of optical thickness, i.e.,

$$\tau_{a\lambda} = \tau_{0.5}\left(\frac{\lambda}{0.5}\right)^{-\alpha}, \quad (1)$$

where the λs are wavelengths given in microns. For determining the value of α, we apply a log-linear fitting at five wavelengths, i.e., $\lambda = 0.400$, 0.500, 0.675, 0.870, and 1.020 μm. In general, α is a basic measure of the aerosol size distribution. For example, small α around zero represents large dust particles whereas large α around 2.0 small smoke particles [*Dubovik et al.*, 2002a].

[17] Mandalgovi shows a large α variation from near zero to 2.0 while AOTs are mostly between near 0 and 1.0. Both mean AOT and its standard deviation (SD) appear to decrease with increased α, and a relatively large variation of AOT can be seen in the lower range of α. As desert dusts over Sahara have lower α from -0.1 to 1.2, and larger AOT from 0.1 to 2.0 [*Tanre et al.*, 2001], the feature suggests that large AOTs and small αs are influenced by dust-like particles. Compared to Mandalgovi, Dunhuang located in the east of the Taklimakan desert shows much smaller α and a wide variation of AOT from near zero to 1.8. Such variations are similar to those found in desert areas of Saudi Arabia and Cape Verde [*Dubovik et al.*, 2002a].

[18] Scatterplots for Yinchuan may be separated into two dominant patterns; one showing an increase of α with increased AOT under relatively wet atmospheric conditions, and the other showing a decrease of α smaller than 0.5 with an increase of AOT from 0.1 to 1.6. The high humidity shown in the former shape suggests that fine particles grow under moist condition with increased AOT. A similar pattern between α and AOT can be seen in urban-industrial aerosols as examined in the Sulfates, Clouds and Radiation-America (SCAR-A) experiment [*Remer et al.*, 1997] and in the Tropospheric Aerosol Radiative Forcing Observational Experiment (TARFOX) [*Hegg et al.*, 1997]. Because Yinchuan is an urban area near the arid region, it is suggested that the former pattern is associated with urban-type aerosols, in which growth of small particles under high humidity conditions is likely one of the possible growing mechanisms [*Kotchenruther et al.*, 1999], as also noted in the strong correlation between AOT and precipitable water content in urban areas [*Holben et al.*, 2001; *Smirnov et al.*, 2000]. On the other hand, the latter pattern is associated with predominant dust particles. *Nakajima et al.* [1989] discussed that air mass mixture of urban aerosols and dust aerosols can produce four characteristic patterns in the α-AOT diagram, i.e., positive correlation with high α value, negative correlation with high α value, negative correlation with low α value, and constant α case.

[19] Among those three sites in arid areas, Dunhuang clearly shows a negative correlation between α and AOT. Such a shape showing smaller α and larger AOT is thought to be associated with soil particles as noted in the work of *Nakajima et al.* [1989] and *Kaufman et al.* [1994]. Considering the fact that all three places are located in/near arid desert regions, a small α with a large AOT must be typical characteristics of Asian dust. Thus dust influences are far more significant in Dunhuang among those three locations.

[20] Sri-Samrong shows two different features separated by about 1.0 of α; one showing a positive relationship between α and AOT when α is larger than 1.0, and the other showing a negative relationship between them. The positive pattern is similar to that found in Yinchuan. Since Sri-Samrong is located in a tropical region, and forest fires frequently occur in the dry season (October to February), such a positive pattern seems to be due to biomass burning, as found similarly in the work of *Eck et al*. [2001]. The α value generally increases and reaches at a peak around 1.7, then levels off with increasing AOT. The leveling-off pattern is also consistent with that found in biomass burning aerosols in the Amazon area [*Eck et al.*, 1999], in Zambia [*Eck et al.*, 2001], and in smokes from boreal forest fires [*Markham et al.*, 1997]. The negative pattern when α is smaller than 1.0 is similar to that found in Dunhuang. Thus we suspect that dust particles are also observed in Sri-Samrong area. In fact, *Sugimoto et al.* [2002] suggested these dust particles could be transported from the northern Indian desert region to the Sri-Samrong area in spring and early summer.

[21] In order to examine seasonal variations of the α-AOT relationship, scatterplots given in Figure 3 are further separated into four seasons, i.e., winter (DJF), spring (MAM), summer (JJA), and fall (SON); see Figure 4. It appears that the atmosphere is more turbid and more variable in the spring and the summer since SD appears large during those seasons. In general, minimum values of mean and standard deviation of AOT are found in the fall.

[22] As shown in Figure 3, Mandalgovi exhibits a large variation of α with smaller AOTs. It is interesting to note that the AOT increases with α when α is larger than 0.5 during the spring and the fall, suggesting that fine particle aerosols are increased in this area during those seasons. Because Mandalgovi is located far from urban areas, the positively correlated pattern between α and AOT during the spring and the fall may be due to the aging processes of coagulation and gas-to-particle conversion without the involvement of high humidity effect. Another candidate to cause such unusually high α values with low AOTs is superfine particles generated by gas-to-particle conversion of biogenic carbonaceous gases emitted from vegetation surrounding the site. The characteristic seasonal variation supports this speculation. On the other hand, dust may also influence the area during the spring and summer. Scatterplots for Dunhuang show a large AOT and a relatively smaller α ($0-1.0$) throughout the year. There is a large variation of AOT when α is smaller than about 0.25 whereas small values of the mean and SD of AOT are noted for α larger than 0.5. Such patterns strongly indicate that Dunhuang is influenced mainly by dust particles all seasons around.

[23] In Yinchuan, there is an indication of AOT increasing with respect to increased α, yet spring (MAM) shows a decreasing trend as well when α is smaller than about 0.5. Thus the main aerosol characteristic in Yinchuan is related to the accumulation process of urban aerosols throughout the year and also due to dusts during the spring.

[24] In Sri-Samrong, α increases with the increased AOT during the winter because of the biomass burning. Such a pattern continues until the rainy season starts in late May. During the rainy season from mid-May to mid-October, the

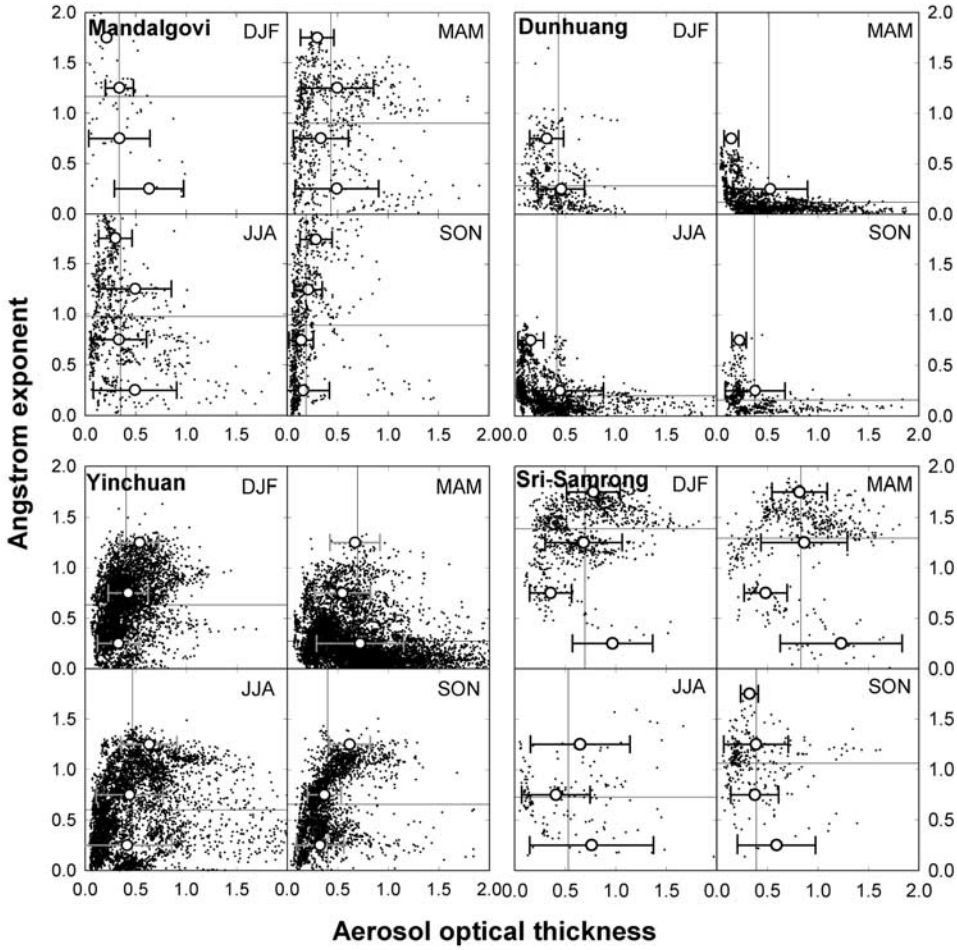

Figure 4. Same as in Figure 3 except instantaneous retrievals for DJF (December–February), MAM (March–May), JJA (June–August), and SON (September–November).

biomass burning pattern seems to disappear, probably due to less chance of biomass burning and the scavenging effect by precipitation. Increasingly, aerosols having larger AOTs with smaller α are also found, especially in MAM, and these α-AOT relationships are somewhat similar to those found in Chinese sites, suggesting the dust influence on Sri-Samrong area. Along with local dust emission, dust particles are expected to be transported from the desert region over the Indian subcontinent following the dominant westerly wind during the spring. Such interpretation is consistent with findings from numerical simulations that the soil dusts are transported from northern Indian arid regions near the Thar desert during April and May [*Takemura et al.*, 2002a, 2002b], and from lidar observations [*Sugimoto et al.*, 2002].

[25] Figure 5 shows the time series of the 10-day mean of derived AOT at 0.5 μm and associated α. There are some gaps in the time series (e.g., October at Dunhuang and May–June at Sri-Samrong), which are mainly due to the fact that atmospheric conditions did not provide enough clear-sky days from which 10-day mean values can be calculated. Other factors for those gaps would be due to the discrepancy between the measured and calculated radiances in the retrieval process, and perhaps due to measurement breaks during the instrument maintenance. We only take 10-day means if the number of observation days is greater than six within the 10-day period, and observation frequencies are greater than 20 a day.

[26] It is found that α values at Mandalgovi show large fluctuations with time, in particular during the spring. From December to the end of March, an out-of-phase relationship between α and AOT is prevalent, and then the relationship turns into in-phase until the end of June. In the latter half of the year, an out-of-phase relationship is noted again, but with smaller AOTs, indicating that very fine particles are prevalent during the spring while a clean air mass is present during the summer and autumn. At Dunhuang, distinct out-of-phase relationships are dominant throughout the year. Low α and relatively high AOT during the period from February to June, and during the fall suggest that Dunhuang is mainly influenced by dusts. It is of interest to note that the seasonal cycle is not evident probably due to the low relative humidity associated with the desert environment and high altitudes above 1000 m. At Yinchuan, an in-phase relationship between AOT and α is noted during the winter, with an out-of-phase relationship during the spring. The out-of-phase relationship again suggests frequent dust storm events influencing the Yinchuan area, but the intensity is weaker and the period is shorter in comparison to those noted in Dunhuang. In Sri-Samrong, two distinct features are found, i.e., showing larger α from mid-September to the end of next spring and

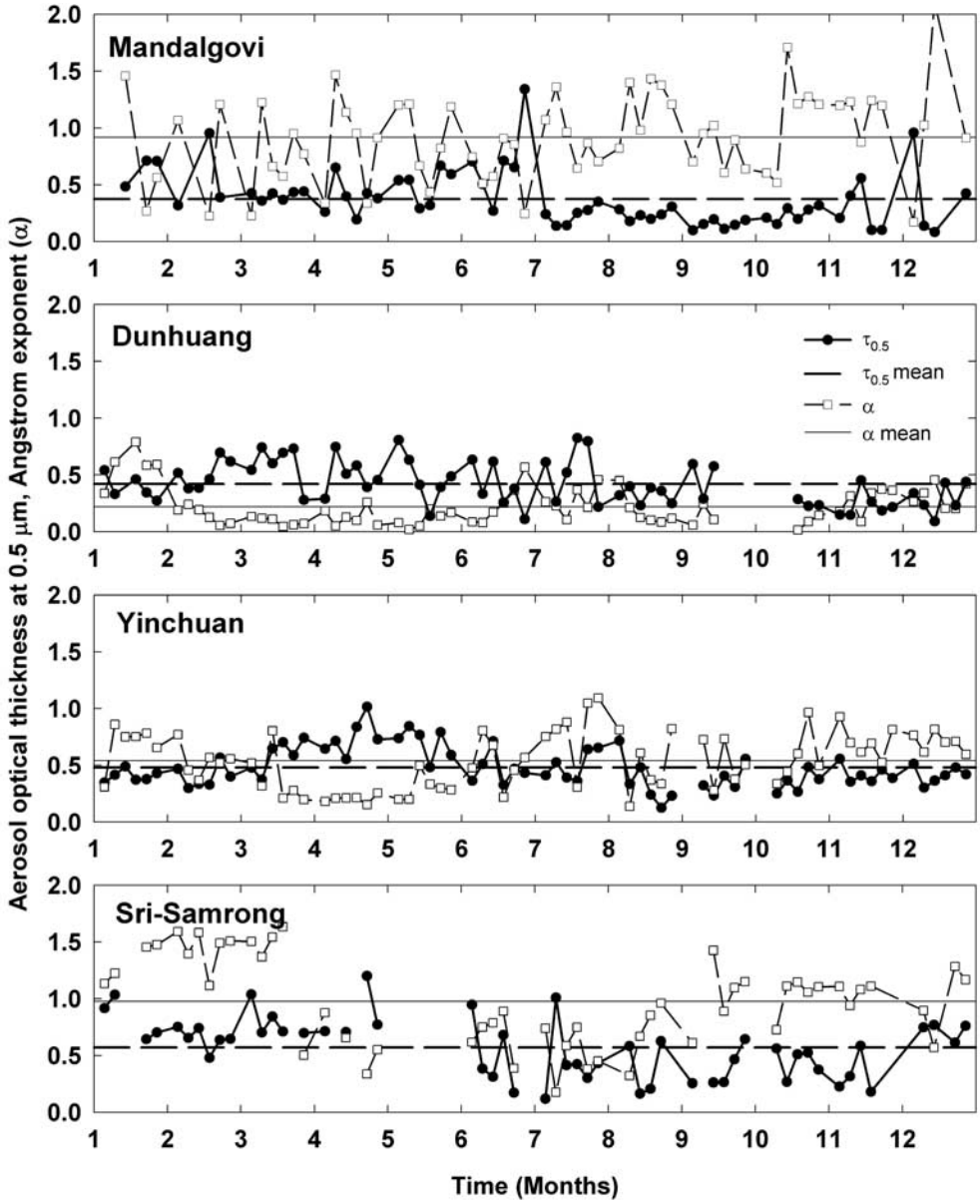

Figure 5. Time series of the 10-day averaged aerosol optical thickness at 0.5 μm (AOT) and Ångström exponent (α). Symbols are given in the second panel.

relatively smaller α for the rest of year. These features seem to come from the meteorological characteristics associated with the seasonal progress of the monsoon system over the Sri-Samrong area. Characteristics found in Sri-Samrong also suggest importance of wind because aerosols can be transported and locally uplifted by winds.

3.1.2. Aerosol Volume Spectrum

[27] Figure 6 shows the monthly average of volume particle size distribution ($dV(r)/d\ln r$ ($cm^3 cm^{-2}$)) obtained from three Chinese sites and one Thailand site. General patterns appear to be bimodal but the mode radius (hereafter the mode is referred to as the volume mode) and total volume exhibit significant variability depending on geography and season.

[28] At Mandalgovi, the fine mode radius is smaller than 0.1 μm, but it shows an increase in the mode radius of the fine mode up to 0.1–0.2 μm in spring and summer. This shift appears to be related to the increases in both AOT and α shown in Figure 4. The largest size difference between fine and coarse modes in Mandalgovi is in coincidence with the largest α range (0.0–2.0), suggesting that various sizes of aerosols exist at Mandalgovi in all seasons around.

[29] In Dunhuang, the fine mode as shown in Mandalgovi almost disappears throughout the year, and thus only coarse mode exists, consistent with large AOT and small α as noted in Figures 3 and 4. The mode radius of the coarse mode around 3–5 μm is found to be larger than other observations of desert dust particles. The AERONET measurements over Saudi Arabia and Cape Verde showed the mode radius of dust particles to be around 2–3 μm [*Dubovik et al.*, 2002a], and 1–5 μm over Saharan dust [*Haywood et al.*, 2001].

[30] Yinchuan shows a fine mode around 0.2 μm and a coarse mode around 5 μm reflecting dominant urban aero-

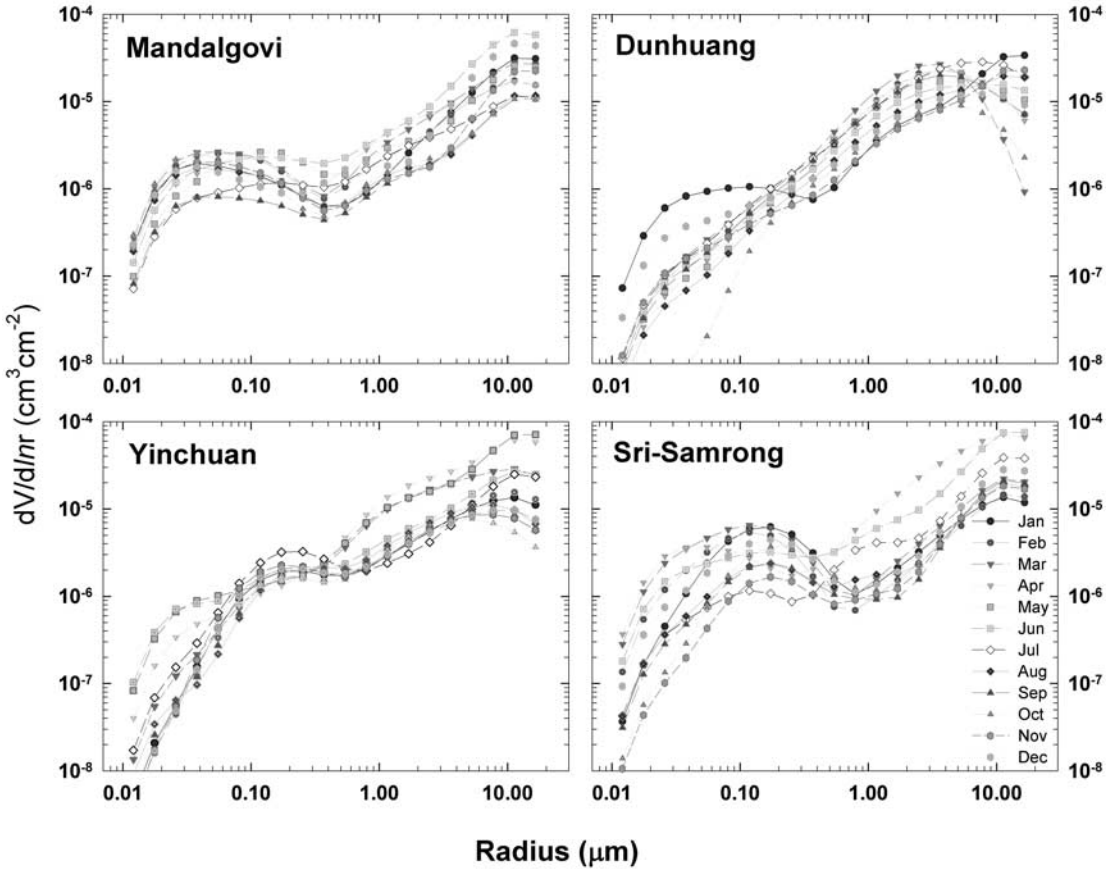

Figure 6. Monthly averaged volume size distributions. Symbols are given in the lower right panel. See color version of this figure in the HTML.

sols in this area. These distributions are in good agreement with measurements for a polluted atmospheric environment [*Dubovik et al.*, 2002a; *Hartley et al.*, 2000; *Remer et al.*, 1997; *Hayasaka et al.*, 1992]. As is typical for aerosols in urban area of northern hemispheric middle latitudes, the total volume of coarse mode particles increases in spring (March to May) forming a weak bimodal pattern.

[31] The mode radius of fine mode at Sri-Samrong is around 0.2 μm, and the total volume of fine mode particles is largest among the sites due to the dominant biomass burning aerosols especially during the winter. It is also of interest to note that the total volume is much increased during April, suggesting dust influence during the spring as shown in Figure 5.

[32] It is worthwhile to note that the total volume of coarse mode particles is always larger than that for fine mode particles at Yinchuan and Sri-Samrong whose respective aerosol types are associated with urban activities and biomass burning. This result showing the larger volume for coarse particles is different from *Dubovik et al.* [2002a] who showed that fine mode particles are dominant volume contributors in urban-industrial and biomass burning areas. Such a difference may be explained by the dust influences from surrounding regions. Yinchuan is situated with the Gobi desert in the north and yellow loess in the southeast, and thus dust particles of radii as large as 10 μm may be easily transported from those surroundings if there is northerly or southeasterly wind. In addition to the dust influence on Sri-Samrong from the Indian subcontinent, the coarse particle mode may be attributed to the surrounding crop-testing fields that sometimes have no vegetation but bare soil in dry season.

3.1.3. Single Scattering Albedo

[33] Spectrally dependent single scattering albedos are retrieved along with an Ångström exponent (β) of $\omega_{a0.5}$ which can be interpreted as the wavelength dependence of single scattering albedo, i.e.,

$$\omega_{a\lambda} = \omega_{a0.5}\left(\frac{\lambda}{0.5}\right)^{-\beta}, \tag{2}$$

where the λs are wavelengths given in microns. Seasonal mean values of $\omega_{a0.5}$ and β at four observation sites are given in Table 1.

[34] Mandalgovi shows the largest value of $\omega_{a0.5}$, 0.92–0.95, among the SKYNET sites, suggesting less absorbing aerosols over Mandalgovi. This is because Mandalgovi is far less influenced by absorbing industrial or biomass burning aerosols, compared with other sites. And a relatively larger value of α and positive β suggest that Mandalgovi is rather influenced by fine particles because of greater scattering of solar radiation by fine particles over the shorter wavelength region.

Table 1. Average of Single Scattering Albedo at 0.5 μm ($\omega_{a0.5}$) and Ångström Exponent of $\omega_{a0.5}$ (β) for DJF (December–February), MAM (March–May), JJA (June–August), and SON (September–November) Periods at SKYNET Sites

	Single Scattering Albedo at 0.5 μm, $\omega_{a0.5}$					Ångström Exponent of $\omega_{a0.5}$, β				
Station	DJF	MAM	JJA	SON	Annual	DJF	MAM	JJA	SON	Annual
Mandalgovi	0.9417	0.9180	0.9379	0.9491	0.9367	0.0434	0.0498	0.0493	0.0540	0.0491
Dunhuang	0.9003	0.9128	0.8963	0.9056	0.9038	−0.0337	−0.0550	−0.0379	−0.0544	−0.0453
Yinchuan	0.9141	0.9047	0.9142	0.9197	0.9132	0.0099	−0.0134	0.0338	0.0275	0.0145
Sri-Samrong	0.9272	0.9201	0.8675	0.9382	0.9133	0.0655	0.0892	0.0040	0.0215	0.0451

[35] Dunhuang shows a relatively smaller seasonal mean $\omega_{a0.5}$ around 0.90, indicating that Asian dusts originated from the Taklimakan desert area absorb a substantial amount of solar radiation which then can give significant impact on aerosol radiative forcing over east Asia. The absorption by Asian dust noted in this study is consistent with reported values from optical retrieval of single scattering albedo [*Dubovik et al.*, 2002a; *Tanre et al.*, 2001; *Carlson and Benjamin*, 1980], but smaller than absorbing characteristics previously recognized by modeling efforts [e.g., *Shettle and Fenn*, 1979; *Hess et al.*, 1998]. Such an agreement with observational results further indicates that dust particles scatter more than previously known. As one of the optical characteristics of aerosols over the Dunhuang area, it can be pointed out that the dust particles near Dunhuang absorb more solar radiation in the shorter wavelength spectrum because of the negative value of the wavelength dependence (β).

[36] At Yinchuan, $\omega_{a0.5}$ is around 0.91 with a minimum in spring. Considering that Yinchuan is an urbanized area which produces much organic carbon, it is interesting to note a smaller scattering albedo compared to that observed over other urban areas, i.e., ~0.98 at 0.44 μm at NASA Goddard Space Flight Center (GSFC), but close to the values from the Indian Ocean Experiment (INDOEX) ranging from 0.86 to 0.9 at 0.55 μm [*Ramanathan et al.*, 2001]. Relatively smaller value of single scattering albedo in Yinchuan and INDOEX area may suggest that soot type aerosols from fossil fuel combustion are more abundant over Asia than over the North American continent. The imaginary index of refraction of urban aerosols in Japan has been retrieved by airborne radiation measurements as from 0.007 to 0.017 over Nagoya [*Tanaka et al.*, 1990], and by polar nephelometry and chemical analysis as from 0.007 to 0.057 at wavelength of 0.5 μm in Sendai with distinct seasonal variation [*Takamura et al.*, 1984; *Hayasaka et al.*, 1992]. *Qiu et al.* [1987] retrieved the imaginary index values from 0.022 to 0.079 with a standard deviation of 0.017 at the wavelength of 0.69 μm from Sun/sky photometry measurements in Beijing, China. These values suggest very low single scattering albedos from 0.5 to 0.93. They explained that the larger imaginary part is due to the coal combustion especially during winter. The increase in fossil fuel burning resulted from economic growth over east Asia would give rise to more emissions of sulfate, organic matter, and soot aerosols into the atmosphere. On the other hand, negative β is only shown during the spring, indicating that Yinchuan is also affected by dust particles during the spring.

[37] Recognizing that major biomass burning in Sri-Samrong area takes place in the winter season, a single scattering albedo of about 0.93 observed during winter period is similar to that from other in situ measurements of AERONET, but somewhat larger. During the summer, because of the rainy season in Sri-Samrong, there may be little chance of biomass burning. Thus much smaller single scattering albedo around 0.87 with a near zero β should be explained by different aerosol forming mechanism. We suspect this is also due to dust particles as shown in α and size distributions of Figures 4 and 6, but it is not clear where they are originated.

[38] We calculated the spectral dependence of ω_a using the ω_a values found in the work of *Tratt et al.* [2001] and *Dubovik et al.* [2002a]. The β values calculated from *Tratt et al.* [2001] ω_a values were 0.049, −0.009, and −0.002 before, during, and after the dust event at San Nicolas Island during April 1998, respectively. The β values calculated from AERONET ground-based radiometers [*Dubovik et al.*, 2002a] are −0.068 for desert dust particles in the Persian Gulf, 0.078 for biomass burning aerosol, and 0.068 for urban industrial aerosols. Thus negative values for Asian dust obtained in this study are consistent with those found for dusts in other areas.

3.2. Characteristics of Asian Dust

[39] During the spring, a large amount of Asian dust is uplifted from northern China and transported to a wide region under prevalent westerlies in midlatitudes. These dusts significantly increase the atmospheric turbidity over east Asia and adjacent Pacific regions in spring, possibly altering the radiation balance over those regions. Moreover, in situ and satellite remote-sensing measurements have shown that dust particles from the Asian continent could be transported beyond the Pacific Ocean to the western seaboard of the United States [*Takemura et al.*, 2002b; *Tratt et al.*, 2001; *Husar et al.*, 2001], indicating that dust influences are not just confined within the surrounding east Asian region. Because of such a vital interest in the possible impact of Asian dusts on local or global climate, there is much need to investigate the optical characteristics of Asian dust particles. In addition to the examination of aerosol characteristics over the dry Dunhuang and Mandalgovi areas, we also use sky radiation measurements at Anmyon and Gosan in Korea, and at Amami-Oshima in Japan for studying the optical properties of Asian dust.

[40] Figure 7 shows the time series of retrieved AOT and Ångström exponent for dust cases. Heavy Asian dust events with AOTs greater than 1.2 are found on 19 April 1998, 7 April 2000, and 26 April 2000 at the Anmyon observation site. During the heavy dust episodes, α was smaller than 0.3 regardless of time. Other Asian dust cases show relatively high AOT from 0.5 to 1.0 and low α around 0.5. On 7 April 2000 at Anmyon, AOT rapidly decreased with time from 2.0 to 0.5 with an increase in α from about 0.0 to 0.3. These large temporal change of AOT can be explained by the fast moving dust band over the Anmyon,

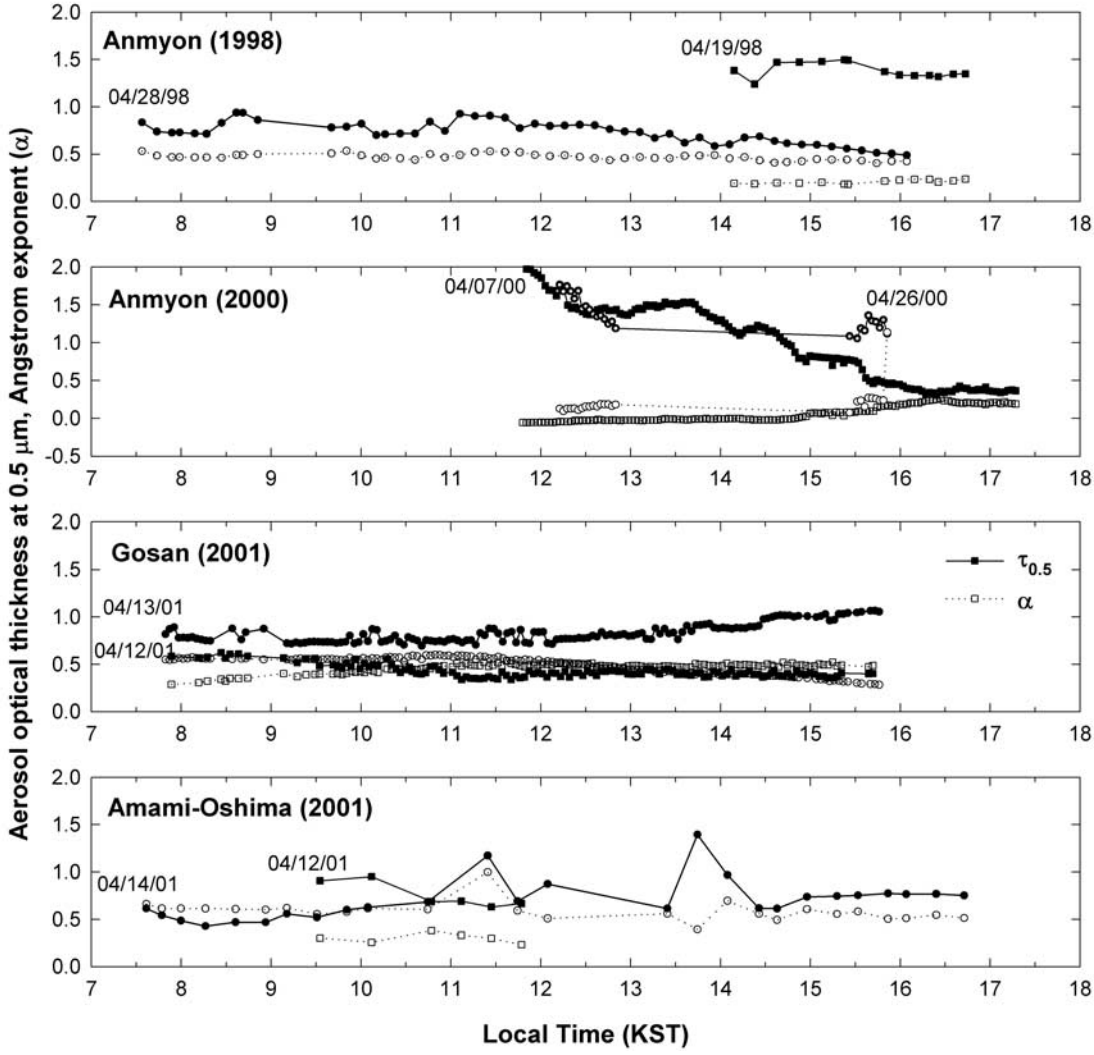

Figure 7. Time series of the aerosol optical thickness at 0.5 μm (AOT) and Ångström exponent (α) for the Asian dust events at Anmyon (April 1998 and 2000), Gosan and Amami-Oshima (April of 2001). Closed and open symbols indicate AOT and α, respectively.

as noted in GMS-5 satellite images displaying the movement of a dust band from the middle part of the peninsula to the south (not shown).

[41] At Gosan, AOTs increased with decreasing α on 12 April 2001. On the other hand, AOTs observed on 13 April 2001 showed a decreasing trend of AOT with time, but nearly invariant α around 0.5. The AOTs and αs at Amami-Oshima are relatively uniform during the observation period except for a few fluctuations.

3.2.1. Aerosol Optical Thickness

[42] Figure 8 shows the scatterplots of daily averaged AOT and α at Anmyon during April of 1998 and 2000, and at Gosan and Amami-Oshima during April of 2001. At Anmyon, various sizes of aerosol particles are observed as seen in the α values ranging from 0.2 to 1.5 with AOT from 0.2 to 1.5. However, dominant aerosols at Anmyon during April exhibit AOTs between 0.2 and 0.6, which represent aerosol properties without dust events.

[43] The largest variations of AOT and α at Anmyon can be explained by the environmental conditions in the vicinity of Anmyon. One power plant is located northwest about 40 km away from the site, so local aerosols emitted from the power plant are likely to be transported into this observation area in addition to continental type aerosols from China under northwesterly conditions. Thus it is not surprising to observe that points showing α values greater than 1.0 appear to have a shape similar to the one found for Yinchuan in Figure 3, reflecting the urban-type aerosols observed in Anmyon. In comparison to the scattered pattern in Anmyon, both Gosan and Amami-Oshima exhibit a general negative relationship between α and AOT during April 2001. The ranges of AOT and α appear to be similar to each other although scattering is larger in Amami-Oshima. For instance, Amami-Oshima shows more points showing more turbid atmospheric conditions. Considering that theses two sites are located in the west coast of the islands and thus less affected by aerosol sources of Korea or Japan under westerly conditions, the more scattered pattern in Amami-Oshima during April suggests that both areas have different generation processes for aerosols interacting

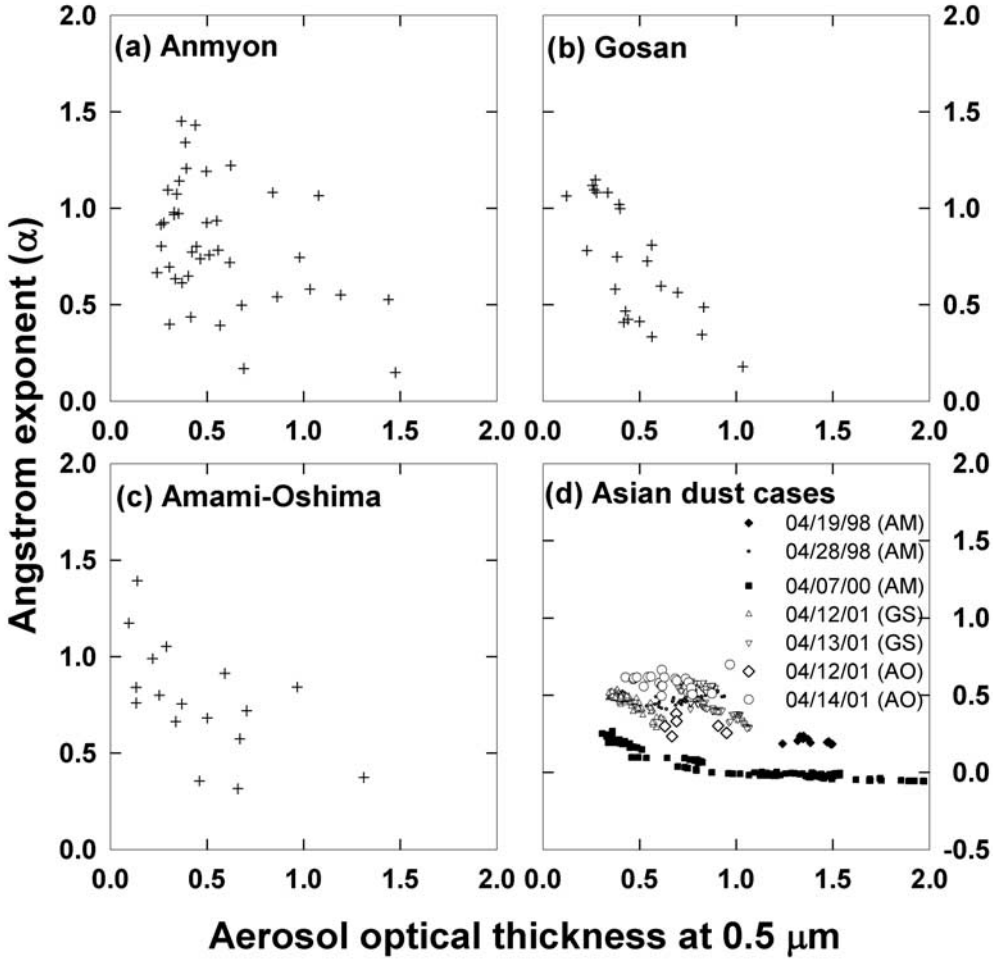

Figure 8. Scatterplots of the aerosol optical thickness at 0.5 μm and Ångström exponent for Anmyon (AM), (b) Gosan (GS), (c) Amami-Oshima (AO), and for (d) Asian dust cases.

with aerosols transported from the continent under the westerlies or northwesterlies in April.

[44] The instantaneous α-AOT relationships for the seven selected Asian dust cases are given in Figure 8d. The scattergram provides the general characteristics defining the Asian dust over the Korean and Japanese areas, i.e., aerosols having α smaller than about 0.6 and AOT larger than 0.3. Thus dust event can be distinguished from the nondust conditions by examining ranges of α and AOT. Furthermore, aerosol types during the dust season can be generally subdivided into three classes with the distribution of α and AOT, i.e., (1) nondust aerosols showing small AOT and various α values ranging from 0.5 to 1.5, (2) light Asian dust case showing relatively large α values around 0.5 but relatively small AOT from 0.5 to 0.8, (3) heavy Asian dust case showing AOTs from 0.5 to 1.5 and α values from −0.05 to 0.3, as shown in the work of *Lee et al.* [2002]. The characteristic α-AOT patterns for these three cases are similar to the four patterns indicated by *Nakajima et al.* [1989]. Another interesting feature is that α values are not as small as zero, which is observed at Dunhuang and Saharan desert regions. As pointed out by aerosol type analysis from satellite [*Higurashi and Nakajima*, 2002], the relatively high α values can be attributed to small accumulation mode aerosols from the continental industrial sources.

3.2.2. Aerosol Volume Spectrum

[45] Figure 9 shows the volume size distribution of Asian dust particles for three sites. At Anmyon, the size distributions show a coarse particle mode at radius of 2–3 μm although the 7 April case shows a mode around 4–5 μm. These values are in quite good agreement with other in situ measurements. *Murayama et al.* [2001] and *Aoki and Fujiyoshi* [2003] showed that the coarse mode radius of Asian dust particles is commonly located around 2–3 μm in Korean and Japanese areas. The optical particle counter measurements also showed distinct increase of large particles around 2–3 μm during Asian dust episodes in April 1998 [*Chun et al.*, 2001; *Husar et al.*, 2001]. Since dust particles larger than 10 μm in radius are preferentially removed by gravitational settling during the movement from the dust source region to Korea or Japan, it may not be common to observe such large particles in the Anmyon area. The dust case on 7 April 2000 shows a significant increase in

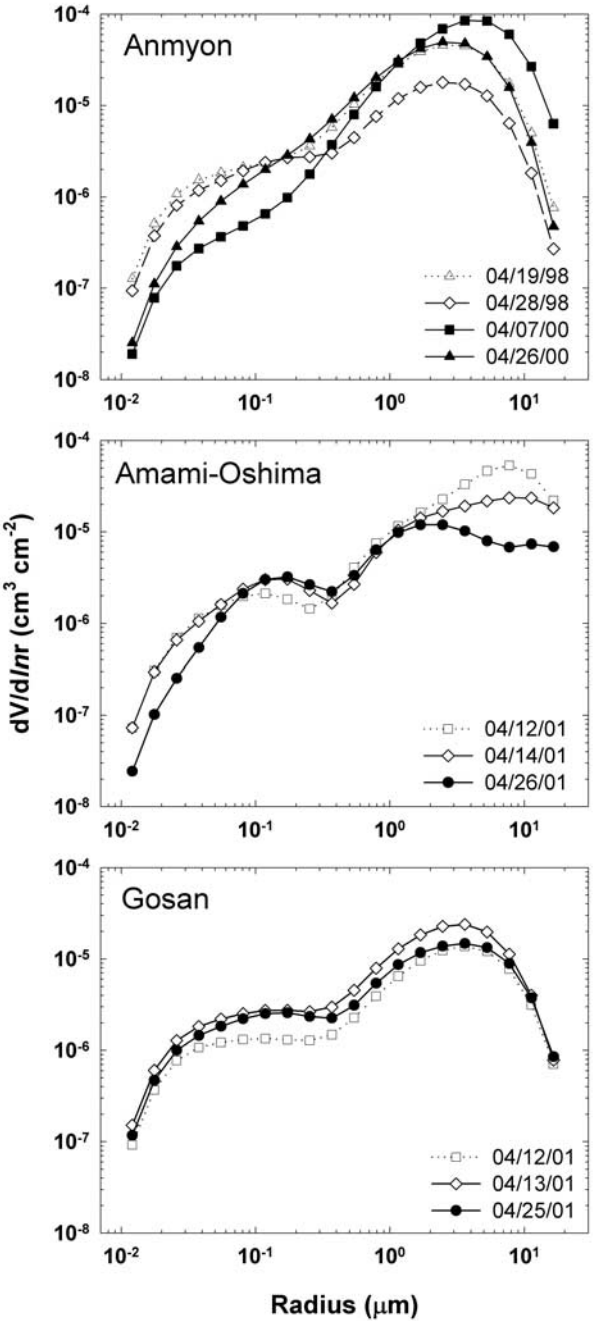

Figure 9. Daily averaged volume size distributions during the Asian dust events at (top) Anmyon, (middle) Gosan, and (bottom) Amami-Oshima.

total volume as seen in a shift of the coarse particle mode to around 4–5 μm and a simultaneous decrease in the total volume of fine mode particles. It is thought that man-made aerosols were less abundant on 7 April because of the frontal passage followed by fast-moving thick dust clouds as suggested in the last subsection.

[46] The retrieved volume distributions for Asian dust observed at Gosan also show a significant number of large particles around 3.0 μm. It is of interest to observe a fine mode in volume around 0.1 μm, which appears to be associated with the effect of man-made aerosols transported from Chinese continent. In comparison to the volume distributions found in Anmyon, dust events observed at Gosan shows a relatively less fluctuating pattern.

[47] In contrast to the less variable patterns noted in Gosan, the dust observations at Amami-Oshima show a much fluctuating pattern, particularly in the coarse mode. A fine mode around 0.1 μm is also found. On 26 April, the coarse particle mode is located at 1.0–2.0 μm, while there is a large increase in the larger particle load between 4.0 and 8.0 μm in radius on 12 and 14 April. Such a difference may not be surprising considering that Amami-Oshima is located far south and thus influenced by different air masses. These results suggest the dust particles up to 10 μm arrive in Amami-Oshima area during the dust season, although the Anmyon and Gosan sites did not exhibit such an increase in volume on account of those large particles. As a matter of fact, *Tanaka et al.* [1989] showed that the mode radius of the coarse particle mode associated with Asian dust outbreak shifts from 2 μm to larger than 10 μm depending on the air mass speed of the dust storm.

[48] To clarify whether the increase in large particles at Amami-Oshima is associated with dust particles, backward trajectory analysis along the isentropic surface was performed for 12 April 2001. Air trajectories were calculated backward from Gosan and Amami-Oshima at 6UTC 12 April 2001 using National Centers for Environmental Predictions (NCEP) reanalysis data. Four times daily temperature and wind data with 2.5 degree spatial resolution on 17 pressure levels are used for calculating isentropic trajectories starting back from two the observation sites. Backward trajectories in Figure 10a are obtained on an isentropic surface of 300.

[49] K over which the movement of Asian dust is well correlated with the general flow of air mass. Further analyses were done using the numerical simulation results of the near-surface aerosol optical thickness from SPRINTARS (Spectral Radiation-Transport Model for Aerosol Species) coupled with a general circulation model [*Takemura et al.*, 2002a, 2002b]. The simulated optical thickness for soil dust aerosols on 12 April 2001 is given in Figure 10b.

[50] The backward trajectory analyses indicate the dust arriving in Gosan and Amami-Oshima originated from different locations in the Gobi desert; the air mass arriving in Amami-Oshima originated from the central-to-west part of the Gobi desert, while the air mass passing through the eastern edge of the desert arrived in Gosan on 12 April. Considering that the west part of Mongolia is the main desert area, the dusts uplifted in that area might carry larger particles into the Amami-Oshima area. Differences in the optical thickness from soil dust aerosols are clear in Figure 10b, which shows higher AOT at Amami-Oshima than in the Gosan area. Thus it is reasonable to interpret that the main mode from 3 to 8 μm found on 12 April 2001 at Amami-Oshima is associated with Asian dust.

3.2.3. Single Scattering Albedo

[51] Figure 11 shows the time series of retrieved single scattering albedo at 0.5 μm ($\omega_{a0.5}$) and the Ångström parameter of $\omega_{a0.5}$ (β) for April. The magnitude of single scattering albedo at Gosan during the dust events is in good agreement with in situ measurements by nephelometer of CMDL (Climate Monitoring and Diagnostics Laboratory)/

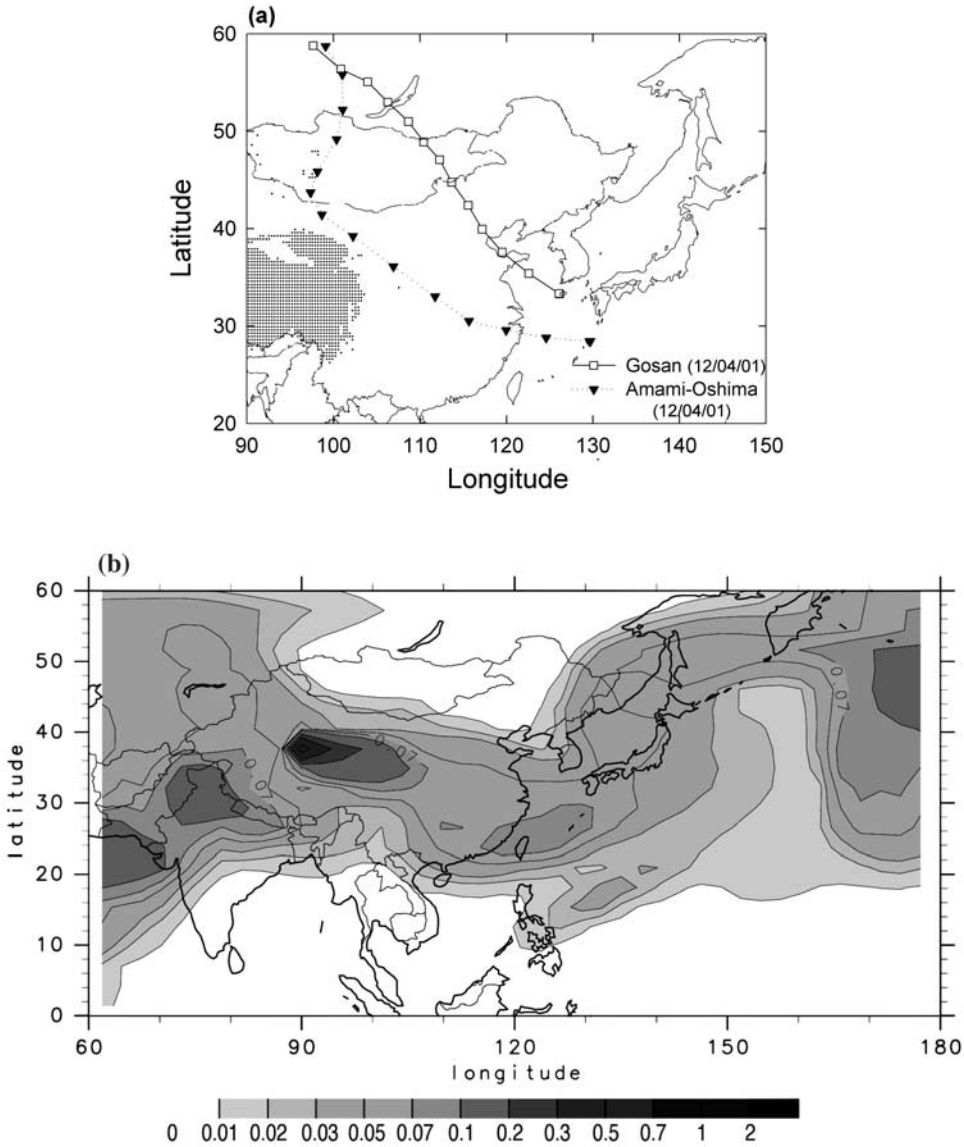

Figure 10. (a) NCEP backward trajectories at Gosan and Amami-Oshima on 12 April 2001. Symbols on the trajectories are given at 6-h time interval. (b) SPRINTARS model results showing optical thickness of soil dust aerosols on 12 April 2001.

NOAA (National Oceanic and Atmospheric Administration) during ACE-Asia in April of 2001 [*Andrews et al.*, 2001]. Single scattering albedos in Amami-Oshima also agree well with nephelometer measurements during APEX [*Ohta et al.*, 2002]. The magnitudes of $\omega_{a0.5}$ around 0.80 at three sites during the Asian dust events are smaller than the value of around 0.9 found in Dunhuang and Yinchuan during spring. This lower single scattering albedo might be due to extensive mixing with polluted air masses containing sulfates and nitrates from China during the dust movement, as most of the aerosol absorption was in the submicrometer particles at Gosan [*Andrews et al.*, 2001], and the concentration of elementary carbon was much increased at Amami-Oshima [*Ohta et al.*, 2002] during Asian dust events.

[52] Importantly the lower single scattering albedo during the Asian dust event suggests the importance of aerosols in climate because the larger absorption effect of the aerosols can significantly alter the radiation balance over the region. They would reduce the downward solar fluxes arriving at the surface, and the reflected solar fluxes at the TOA. Thus the dust particles may have exerted a significant cooling effect on surface radiative forcing but a warming effect at the TOA, due to the increased absorption of solar energy within the atmosphere.

4. Conclusions

[53] The aerosol properties showing seasonal and geographical variations over east Asia were investigated by sky radiation measurements at SKYNET sites. Also included are measurements at Anmyon, Gosan in Korea and Amami-Oshima in Japan during the Asian dust seasons for examining the optical characteristics of Asian dusts over the Korean and Japanese areas.

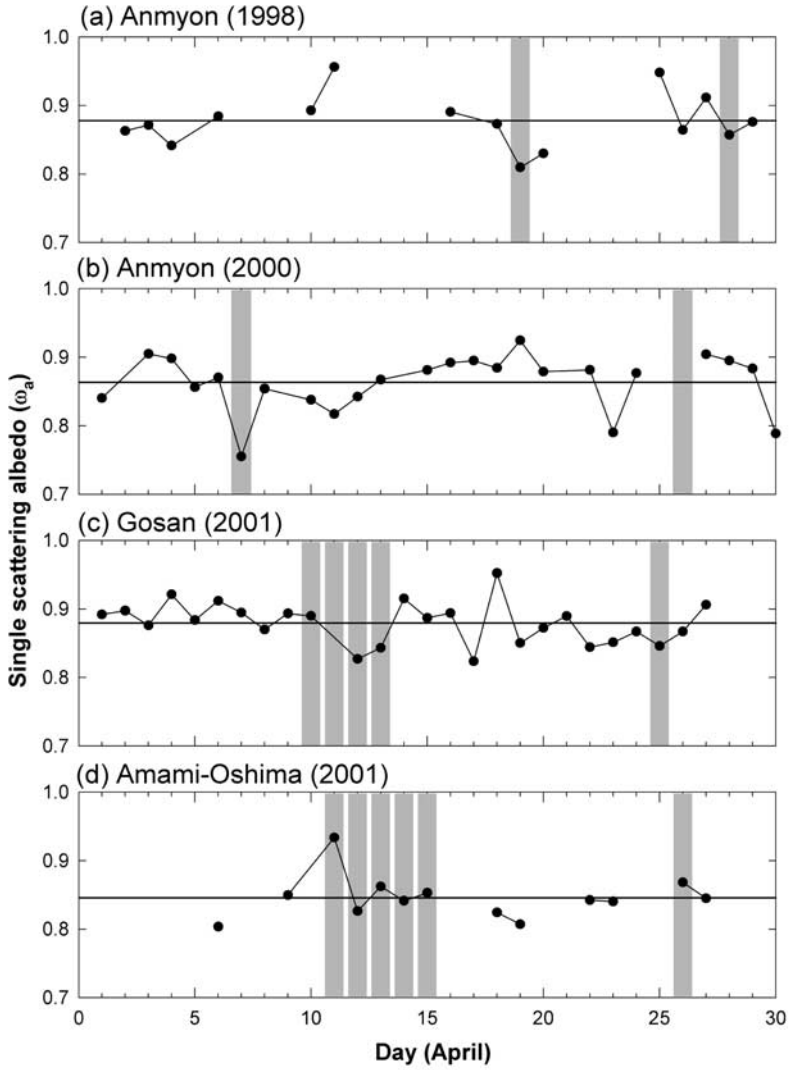

Figure 11. Time series of single scattering albedo at 0.5 μm ($\omega_{a0.5}$) for Anmyon on (a) April 1998, and (b) April 2000, (c) Gosan, and (d) Amami-Oshima on April 2001.

[54] Various kinds of aerosols, such as dust, urban polluted, and biomass burning aerosols exist according to geography and season. As most areas are commonly influenced by dust particles, AOT over east Asia generally shows larger values compared to those found in North America or Europe. Mandalgovi has large α range (0–2.0) due to the fine mode, but there also exist dust particles during the spring and summer. Dust particles are main aerosols all seasons around at Dunhuang. Yinchuan is influenced by urban polluted aerosols throughout the year, but by dust particles in spring. Although mostly affected by biomass burning at Sri-Samrong, we could also find the signals related to dust particles transported from Indian arid region during April and May.

[55] Volume spectra of Dunhuang and Mandalgovi mostly show coarse mode particles in all seasons although Mandalgovi showed an additional fine mode smaller than 0.1 μm in radius. On the other hand, both Sri-Samrong and Yinchuan showed fine modes around 0.1–0.2 μm, suggesting that both regions are under polluted atmospheric environment, respectively, by biomass burning and fuel combustion.

[56] The single scattering albedos of dust particles over east Asia are around 0.9 at 0.5 μm in the arid Dunhuang and Mandalgovi sites, which are larger than the previously known single scattering albedo for mineral dusts. However, those values are quite similar to those found in the AERONET analysis for Saharan desert. The biomass burning aerosols at Sri-Samrong have a relatively larger single scattering albedo around 0.92–0.94.

[57] Asian dust particles found in Korean and Japanese areas appear to have quite different characteristics depending on the latitudes of the sites, which in effect should be closely linked to different dust origins and mixing processes. The single scattering albedos around 0.80 during the dust events are found to be smaller than those observed in source regions. These findings strongly suggest that industrial or urban aerosols transported from eastern China under the westerlies may significantly affect aerosol properties during the dust events through the mixing processes.

These could change the intensity of aerosol radiative forcing substantially at the surface and the TOA over the east Asian region.

Appendix A

A1. Inversion Algorithm and Uncertainty Analysis

[58] Detailed description of the inversion algorithm for aerosol optical thickness and volume distribution are found in the work of *Nakajima et al.* [1996]. In this section we briefly summarize the retrieval method and provide some results from the sensitivity test taken for uncertainty analysis.

[59] The monochromatic direct sky flux density F (W m^{-2} μm^{-1}) is given by

$$F = F_0 \exp(-m_0 \tau) \tag{A1}$$

where F_o is the flux at the top the atmosphere, τ is the total optical thickness, and m_o is the optical air mass, $m_o = 1/\cos\theta_o$. The monochromatic diffuse sky flux density $E(\Theta)$ (W m^{-2} μm^{-1}) is determined as the solution of the radiative transfer equation, i.e.,

$$E(\Theta) = F m_0 \Delta\Omega [\omega\tau P(\Theta) + q(\Theta)] \tag{A2}$$

where ω is the single scattering albedo of the whole air mass, $P(\Theta)$ is the total phase function at a scattering angle Θ, $\Delta\Omega$ is the solid angle of the sky radiometer, and $q(\Theta)$ represents the contribution from multiple scattering. For the inversion retrieval, we use a relative intensity $R(\Theta)$ - the ratio of the diffuse sky flux to the direct flux - since $R(\Theta)$ can be measured more accurately than $E(\Theta)$. Then

$$R(\Theta) = \frac{E(\Theta)}{F m_0 \Delta\Omega} = \omega\tau P(\Theta) + q(\Theta) = \beta(\Theta) + q(\Theta) \tag{A3}$$

The ratio $R(\Theta)$ is less affected by deterioration of the interference filters, thus it is very useful for long-term monitoring. When voltage outputs for F, F_o, and E are given by L, L_o, and L_E, respectively, equations (A2) and (A3) can be expressed as:

$$L = L_0 \exp(-m\tau_{t\lambda}), R(\Theta) = \frac{L_E(\Theta)}{L m_0 \Delta\Omega} = \beta(\Theta) + q(\Theta) \tag{A4}$$

Calibration coefficients for L_o and $\Delta\Omega$ are necessary before applying the inversion scheme. L_o can be obtained by using an improved Langley method that gives better correlation coefficients than a normal Langley method [*Tanaka et al.*, 1986; *Nakajima et al.*, 1996]. $\Delta\Omega$ is determined by the disk scanning method [*Nakajima et al.*, 1996].

A2. Aerosol Optical Thickness

[60] The aerosol optical thickness, $\tau_a(\lambda)$, is defined as:

$$\tau_a(\lambda) = \frac{2\pi}{\lambda} \int_{r_{\min}}^{r_{\max}} K_{ext}(x, \tilde{m}) v(r) d\ln r \tag{A5}$$

In equation (A5), $x(= 2\pi r/\lambda)$ is the size parameter, $v(r)$ $(= dV/d\ln r$ $(cm^3$ $cm^{-2}))$ is the columnar volume spectrum. $r_{\min}$ and $r_{\max}$ are minimum and maximum aerosol radii, respectively, and $\tilde{m}$ is the aerosol complex refractive index. The kernel function K_{ext} is defined as:

$$K_{ext}(x, \tilde{m}) = \frac{3}{4} \frac{Q_{ext}(x)}{x} \tag{A6}$$

where Q_{ext} is the extinction efficiency as given by Mie theory for spherical particles.

A3. Volume Spectrum

[61] Columnar volume spectrum is defined as the volume of aerosols loaded in an atmospheric column, given with logarithmic radius intervals, i.e.,

$$\frac{dV}{d\ln r} = \frac{V_0}{\sigma\sqrt{2\pi}} \exp\left[-\frac{(\ln(r/r_m))^2}{2\sigma^2}\right] \tag{A7}$$

where $dV/d\ln r$ is the volume distribution, V_o is the volume of the particles per cross section of the atmospheric column, and r, r_m, σ represent radius, volume mode radius, and standard deviation of the particles, respectively. The aerosol differential scattering coefficient (β_A) can be expressed as:

$$\beta_A(\Theta) = (2\pi/\lambda) \int_{r_{\min}}^{r_{\max}} K(\Theta, x, \tilde{m}) v(r) d\ln r \tag{A8}$$

$$K(\Theta, x, \tilde{m}) = \left(\frac{3}{2}\right) \frac{i_1 + i_2}{x^3}$$

where K is the kernel function. The aerosol volume radius distribution [$v(r)$] is derived from $\beta_A(\Theta)$ and τ_a of equation (A8) using the iterated inversion schemes.

A4. Single Scattering Albedo

[62] The extinction coefficient can be expressed as the sum of scattering and absorption coefficients, so single scattering albedo (ω_λ) is given by

$$\omega_\lambda = \frac{\sigma_s(\lambda)}{\sigma_e(\lambda)} = 1 - \frac{\sigma_a(\lambda)}{\sigma_e(\lambda)} \tag{A9}$$

where $\sigma_e(\lambda)$, $\sigma_a(\lambda)$, and $\sigma_s(\lambda)$ represent coefficients for extinction, absorption, and scattering, respectively. Aerosol optical thickness for the scattering ($\tau_{sca}(\lambda)$) can be obtained by substituting $K_{sca}(x, \tilde{m})$ for $K_{ext}(x, \tilde{m})$ in the inversion procedure using a similar equation to equation (A5). The complex refractive index is invariant with wavelength in the version 3 of the algorithm [*Nakajima et al.*, 1996], and is composed of 8 prior values for both real and imaginary part in the kernel matrix. Optimal value of refractive index is retrieved by iterative method satisfying the error criterion in equation (A11). Thus complex refractive index ($\tilde{m}$) should be retrieved together with aerosol volume size distribution ($v(r)$) preferentially, and then single scattering albedo (ω_λ) is determined by

$$\omega_\lambda = \frac{\tau_{sca}(\lambda)}{\tau_a(\lambda)} \tag{A10}$$

Inversions are solved if the difference between observed and calculated radiance (Err) is smaller than 0.07 in the final loop of retrieval procedure.

$$\mathrm{Err} = \sqrt{\frac{\sum^{n} \left({}^{R_C}/_{R-1}\right)^2}{n}} \tag{A11}$$

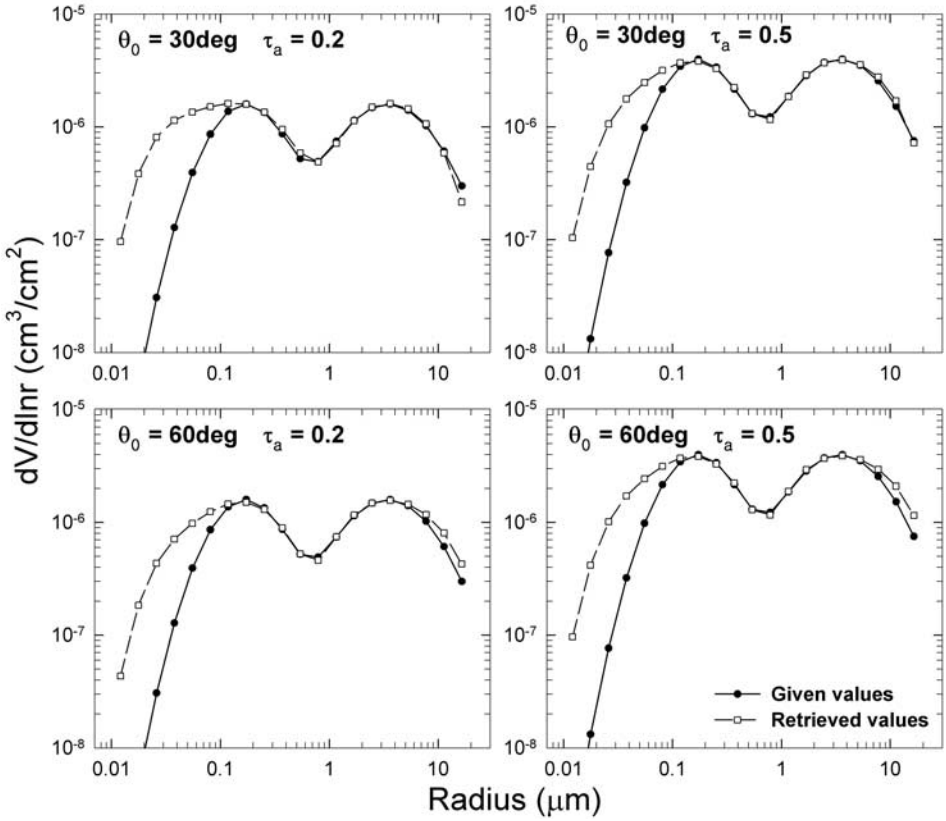

Figure A1. The retrieved size distribution versus given size distribution in error-free conditions for the given solar zenith angle and aerosol optical thickness.

where R_c is the calculated value from retrieved parameters. The inversion procedure is terminated whenever Err is larger than the preset value of 1.0.

A5. Sensitivity Test

[63] In order to assess the algorithm performance, we first simulate $R(\Theta)$ under the conditions of $\tilde{m} = 1.5 - 0.01i$, $r_{min} = 0.01$ μm, $r_{max} = 20$ μm, surface albedo = 0.1, aerosol optical thickness at 0.5 μm (four types in this study: 0.05, 0.2, 0.5, and 1.0), and solar zenith angles (two types: $\theta_o = 30°$, and 60°). In this simulation, a lognormal volume distribution with fine ($r_1 = 0.17$ μm) and coarse ($r_2 = 3.44$ μm) mode radii is assumed. Then we retrieve the aerosol properties from the simulated $R(\Theta)$.

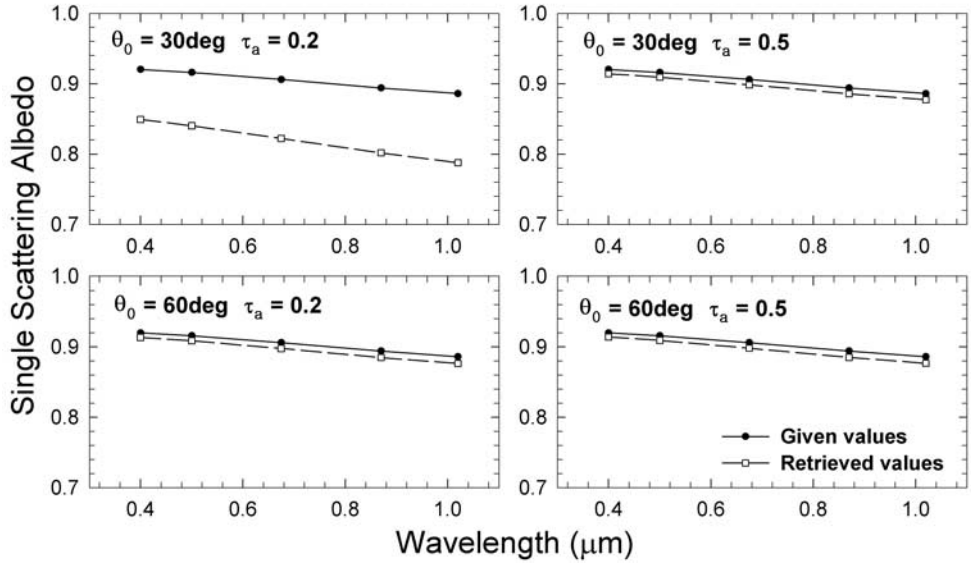

Figure A2. Same as Figure A1 except single scattering albedo.

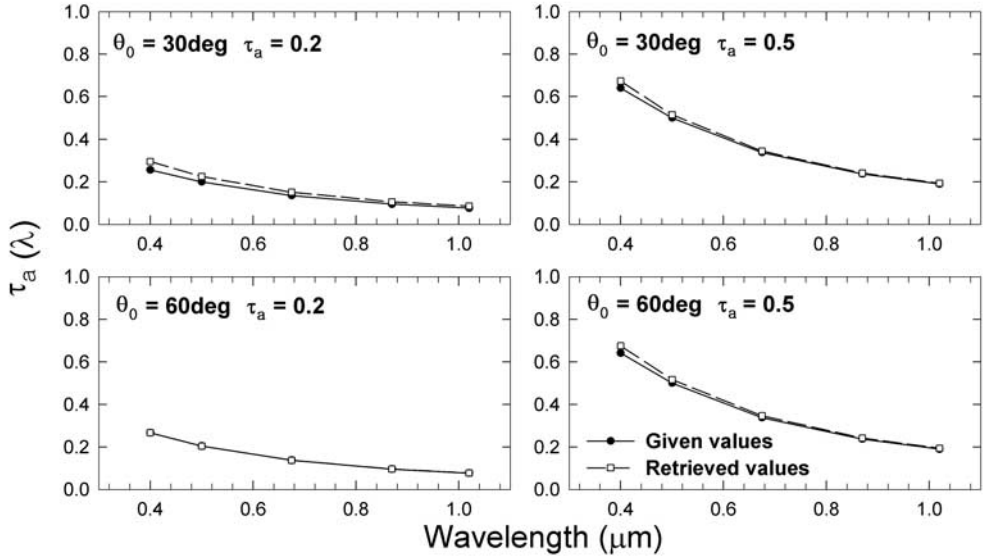

Figure A3. Same as Figure A1 except aerosol optical thickness.

[64] Figure A1 shows the volume spectra retrieved from simulated and given volume spectra. It is noted that the difference between the given distribution and the retrieved distribution becomes significantly large when particle sizes are smaller than 0.1 μm. On the other hand, it appears that the difference for large particles greater 10 μm is not as large as small particles. Results suggest that particles whose radii are between 0.1 and 10 μm can be retrieved with an acceptable accuracy using the inversion approach provided in this section.

[65] Figure A2 shows single scattering albedo as a function of wavelength. It appears that the algorithm tends to underestimate the single scattering albedo, however, the difference between given value and retrieved single scattering albedo seems to be minimal if aerosols are thick or solar zenith angle is large. By the same token, considering the fact that the difference reaches up to 0.08 when both solar zenith angle and optical thickness become lower (in this study $\theta_o = 30°$ and $\tau_{0.5} = 0.2$), caution must be exercised to interpret the retrieved single scattering albedo from the measurements taken under such conditions.

[66] The retrieved aerosol optical thickness is given in Figure A3 as a function of wavelength, along with given optical thickness. Figure A3 shows that the differences between given optical thickness and retrieved values are as large as 0.02 at 0.5 μm, suggesting that the optical thickness retrievals are more accurate.

[67] **Acknowledgments.** The authors would like to thank two anonymous reviewers for their constructive and valuable comments, which led to an improved version of the manuscript. This research has been supported by the Climate Environment System Research Center sponsored by the SRC Program of Korea Science and Engineering Foundation, by the BK21 Project of the Korean Government, and also by the APEX Project of Japan Science and Technology Corporation. Part of this research was performed while the first author was hosted by the CCSR as a visiting scientist.

References

Andrews, E., D. Delence, D. Jackson, A. Jefferson, J. Ogren, P. Sheridan, and J. Wendell (2001), *Clim. Monit. and Diagn. Lab. Summ. Rep.*, *26*, pp. 60–79, Clim. Monit. and Diagn. Lab., Boulder, Colo.

Aoki, K., and Y. Fujiyoshi (2003), Sky radiometer measurements of aerosol optical properties over Sapporo, Japan, *J. Meteorol. Soc. Jpn.*, *81*, 493–513.

Carlson, T. N., and S. G. Benjamin (1980), Radiative heating rates for Saharan dust, *J. Atmos. Sci.*, *37*, 193–213.

Chameides, W. L., et al. (1999), Case study of the effects of atmospheric aerosols and regional haze on agriculture: An opportunity to enhance crop yields in China through emission controls, *Proc. Natl. Acad. Sci.*, *96*, 13,626–13,633.

Cho, H. K. (1981), The variation of atmospheric turbidity over Seoul, *J. Kor. Meteorol. Soc.*, *17*, 1–21.

Chun, Y. S., K. O. Boo, J. Y. Kim, S. U. Park, and M. H. Lee (2001), Synopsis, transport, and physical characteristics of Asian dust in Korea, *J. Geophys. Res.*, *106*, 18,461–18,469.

Dubovik, O., A. Smirnov, B. N. Holben, M. D. King, Y. J. Kaufman, T. F. Eck, and I. Slutsker (2000), Accuracy assessment of aerosol optical properties retrieved from Aerosol Robotic Network (AERONET) Sun and sky radiance measurements, *J. Geophys. Res.*, *105*, 9791–9806.

Dubovik, O., B. N. Holben, T. F. Eck, A. Smirnov, Y. J. Kaufman, M. D. King, D. Tanre, and I. Slutsker (2002a), Variability of absorption and optical properties of key aerosol types observed in worldwide locations, *J. Atmos. Sci.*, *59*, 590–608.

Dubovik, O., B. N. Holben, T. Lapyonok, A. Sinyuk, M. I. Mishchenko, P. Yang, and I. Slutsker (2002b), Non-spherical aerosol retrieval method employing light scattering by spheroids, *Geophys. Res. Lett.*, *29*(10), 1415, doi:10.1029/2001GL014506.

Eck, T. F., B. N. Holben, J. S. Reid, O. Dubovik, A. Smirnov, N. T. O'Neill, I. Slutsker, and S. Kinne (1999), Wavelength dependence of the optical depth of biomass burning, urban and desert dust aerosols, *J. Geophys. Res.*, *104*, 31,333–31,350.

Eck, T. F., B. N. Holben, D. E. Ward, O. Dubovik, J. S. Reid, A. Smirnov, M. M. Mukelabai, N. C. Hsu, N. T. O'Neill, and I. Slutsker (2001), Characterization of the optical properties of biomass burning aerosols in Zambia during the 1997 ZIBBEE field campaign, *J. Geophys. Res.*, *106*, 3425–3448.

Hartley, W. S., P. V. Hobbs, J. L. Ross, P. B. Russell, and J. M. Livingston (2000), Properties of aerosols aloft relevant to direct radiative forcing off the mid-Atlantic coast of the United States, *J. Geophys. Res.*, *105*, 9859–9885.

Hayasaka, T., T. Nakajima, S. Ohta, and M. Tanaka (1992), Optical and chemical properties of urban aerosols, *Atmos. Environ., Part A*, *26*, 2055–2062.

Haywood, J. M., and V. Ramaswamy (1998), Global sensitivity studies of the direct radiative forcing due to anthropogenic sulfate and black carbon aerosols, *J. Geophys. Res.*, *103*, 6043–6058.

Haywood, J. M., P. N. Francis, M. D. Glew, and J. P. Taylor (2001), Optical properties and direct radiative effect of Saharan dust: A case study of two Saharan dust outbreaks using aircraft data, *J. Geophys. Res.*, *106*, 18,417–18,430.

Hegg, D. A., J. Livingston, P. V. Hobbs, T. Novakov, and P. B. Russell (1997), Chemical apportionment of aerosol column optical depth off the

mid-Atlantic coast of the United States, *J. Geophys. Res.*, *102*, 25,293–25,303.

Hess, M., P. Koepke, and I. Schult (1998), Optical properties of aerosols and clouds: The software package OPAC, *Bull. Am. Meteorol. Soc.*, *79*, 831–844.

Higurashi, A., and T. Nakajima (2002), Detection of aerosol types over the East China Sea near Japan from four-channel satellite data, *Geophys. Res. Lett.*, *29*(17), 1836, doi:10.1029/2002GL015357.

Holben, B. N., et al. (2001), An emerging ground-based aerosol climatology: Aerosol optical depth from AERONET, *J. Geophys. Res.*, *106*, 12,067–12,097.

Husar, R. B., et al. (2001), Asian dust events of April 1998, *J. Geophys. Res.*, *106*, 18,317–18,330.

Intergovernmental Panel on Climate Change (IPCC) (2001), *Climate Change 2001, The Scientific Basis*, edited by J. T. Houghton et al., 881 pp., Cambridge Univ. Press, New York.

Jacobson, M. Z. (2001), Strong radiative heating due to the mixing state of black carbon in atmospheric aerosols, *Nature*, *409*, 695–697.

Kaufman, Y. J., A. Gitelson, A. Karnieli, E. Ganor, R. S. Fraser, T. Nakajima, S. Mattoo, and B. N. Holben (1994), Size distribution and scattering phase function of aerosol particles retrieved from sky brightness measurements, *J. Geophys. Res.*, *99*, 10,341–10,356.

Kotchenruther, R., P. V. Hobbs, and D. A. Hegg (1999), Humidification factors for atmospheric aerosols off the mid-Atlantic coast of the United States, *J. Geophys. Res.*, *104*, 2239–2251.

Lee, S. S., B. J. Sohn, D. S. Shin, H. Fukushima, and T. Nakajima (2002), Optical characteristics of the Asian dust aerosol from sky radiation measurements in spring 1998, *Kor. J. Atmos. Sci.*, *5*, 161–170.

Markham, B. L., J. S. Schafer, B. N. Holben, and R. N. Halthore (1997), Atmospheric aerosol and water vapor characteristics over north central Canada during BOREAS, *J. Geophys. Res.*, *102*, 29,737–29,745.

Murayama, T., et al. (2001), Ground-based network observation of Asian dust events of April 1998 in east Asia, *J. Geophys. Res.*, *106*, 18,345–18,360.

Nakajima, T., M. Tanaka, M. Yamano, M. Shiobara, K. Arao, and Y. Nakanishi (1989), Aerosol optical characteristics in the yellow sand events observed in May, 1982 in Nagasaki, part II: Model, *J. Meteorol. Soc. Jpn.*, *67*, 279–291.

Nakajima, T., G. Tonna, R. Rao, R. Boi, Y. Kaufman, and B. Holben (1996), Use of sky brightness measurements from ground for remote sensing of particulate polydispersions, *Appl. Opt.*, *35*, 2672–2686.

Nakajima, T., A. Higurashi, K. Kawamoto, and J. E. Penner (2001), A possible correlation between satellite-derived cloud and aerosol microphysical parameters, *Geophys. Res. Lett.*, *28*, 1171–1174.

Nakajima, T., et al. (2003), Significance of direct and indirect radiative forcings of aerosols in the East China Sea region, *J. Geophys. Res.*, *108*(D23), 8658, doi:10.1029/2002JD003261, in press.

Ohta, S., K. Ryo, M. Naoto, and Y. Sadamu (3–5 June 2002), Measurements of optical and chemical properties of atmospheric aerosols at Fukue and Amami-Oshima islands, paper presented at 5th APEX International Workshop, Jpn. Sci. and Technol. Corp., Miyazaki, Japan.

Qiu, J., Z. Xiuji, S. Jinhui, X. Qilin, and Z. Jinding (1987), Simultaneous determination of the aerosol size distribution, refractive index, and surface albedo from radiance data, in *Atmospheric Radiation: Progress and Process*, edited by K.-N. Liou and Z. Xiuji, pp. 550–556, Science Press, London.

Ramanathan, V., et al. (2001), Indian Ocean Experiment: An integrated analysis of the climate forcing and effects of the great Indo-Asian haze, *J. Geophys. Res.*, *106*, 28,371–28,398.

Remer, L. A., D. A. Hegg, Y. J. Kaufman, and B. N. Holben (1997), Urban/industrial aerosol: Ground-based Sun/sky radiometer and airborne in situ measurements, *J. Geophys. Res.*, *102*, 16,849–16,859.

Russell, P. B., J. M. Livingston, P. Hignett, S. Kinne, J. Wong, A. Chien, R. Bergstrom, O. Durkee, and P. V. Hobbs (1999), Aerosol-induced radiative flux changes off the United States mid-Atlantic coast: Comparison of values calculated from Sun photometer and in situ data with those measured by airborne pyranometer, *J. Geophys. Res.*, *104*, 2289–2307.

Satheesh, S. K., V. Ramanathan, X. Li-Jones, J. M. Lobert, I. A. Podgorny, J. M. Prospero, B. N. Holben, and N. G. Loeb (1999), A model for the natural and anthropogenic aerosols over the tropical Indian Ocean derived from Indian Ocean Experiment data, *J. Geophys. Res.*, *104*, 27,421–27,440.

Shettle, E. P., and R. W. Fenn (1979), Models for the aerosols of the lower atmosphere and the effects of humidity variations on their optical properties, *AFGL-TR-79-0214*, 94 pp., Air Force Geophys. Lab., Hanscom Air Force Base, Mass.

Shiobara, M., T. Hayasaka, T. Nakajima, and M. Tanaka (1991), Aerosol monitoring by use of a scanning spectral radiometer in Sendai, Japan, *J. Meteorol. Soc. Jpn.*, *69*, 57–70.

Smirnov, A., B. N. Holben, T. F. Eck, O. Dubovik, and I. Slutsker (2000), Cloud-screening and quality control algorithms for the AERONET database, *Remote Sens. Environ.*, *73*, 337–349.

Sokolik, I. N., and O. B. Toon (1999), Incorporation of mineralogical composition into models of the radiative properties of mineral aerosol from UV to IR wavelengths, *J. Geophys. Res.*, *104*, 9423–9444.

Sugimoto, N., A. Shimizu, and I. Matsui (3–5 June 2002), Observations of aerosols and clouds with lidars, paper presented at 5th APEX International Workshop, Miyazaki, Japan.

Takamura, T., M. Tanaka, and T. Nakajima (1984), Effects of atmospheric humidity on the refractive index and the size distribution of aerosols as estimated from light scattering measurements, *J. Meteorol. Soc. Jpn.*, *62*, 573–582.

Takemura, T., T. Nakajima, O. Dubovik, B. N. Holben, and S. Kinne (2002a), Single-scattering albedo and radiative forcing of various aerosol species with a global three-dimensional model, *J. Clim.*, *15*, 333–352.

Takemura, T., I. Uno, T. Nakajima, A. Higurashi, and I. Sano (2002b), Modeling study of long-range transport of Asian dust and anthropogenic aerosols from east Asia, *Geophys. Res. Lett.*, *29*(24), 2158, doi:10.1029/2002GL016251.

Tanaka, M., T. Nakajima, and M. Shiobara (1986), Calibration of a sunphotometer by simultaneous measurements of direct-solar and circumsolar radiations, *Appl. Opt.*, *25*, 1170–1176.

Tanaka, M., T. Nakajima, M. Shiobara, M. Yamano, and K. Arao (1989), Aerosol optical characteristics in the yellow sand events observed in May, 1982 in Nagasaki, part I: Observation, *J. Meteorol. Soc. Jpn.*, *67*, 267–278.

Tanaka, M., T. Hayasaka, and T. Nakajima (1990), Airborne measurements of optical properties of tropospheric aerosols over an urban area, *J. Meteorol. Soc. Jpn.*, *68*, 335–345.

Tanre, D., Y. J. Kaufman, B. N. Holben, B. Chatenet, A. Karnieli, F. Lavenu, L. Blarel, O. Dubovik, L. A. Remer, and A. Sminov (2001), Climatology of dust aerosol size distribution and optical properties derived from remotely sensed data in the solar spectrum, *J. Geophys. Res.*, *106*, 18,205–18,217.

Tratt, D. M., R. J. Frouin, and D. L. Westphal (2001), April Asian dust event: A southern California perspective, *J. Geophys. Res.*, *106*, 18,371–18,379.

van Aardenne, J. A., G. R. Carmichael, H. Levy II, D. Streets, and L. Hordijk (1999), Anthropogenic NOx emissions in Asia in the period 1990–2020, *Atmos. Environ.*, *33*, 633–646.

B.-C. Choi, Korea Global Atmosphere Watch Observatory (KGAWO), Meteorological Research Institute (METRI)/KMA, 1764-6, Seungen-Ri, Anmyeon-Up, Taean-Kun, Chung-Nam 357-961, Korea. (cbc@kma.go.kr)

D.-H. Kim, B.-J. Sohn, and S.-C. Yoon, School of Earth and Environmental Sciences, Seoul National University, Mailcode NS80, Seoul 151–747, Korea. (kimdh@eosat.snu.kr; sohn@snu.ac.kr; yoon@snu.ac.kr.)

T. Nakajima, Center for Climate System Research, University of Tokyo, 4-6-1 Komaba, Meguro-ku, Tokyo 153-8904, Japan. (teruyuki@ccsr.u-tokyo.ac.jp)

T. Takamura, Center for Environmental Remote Sensing, Chiba University, 1-33 Yayoi-cho, Inage-ku, Chiba 263-8522, Japan. (takamura@ceres.cr.chiba-u.ac.jp)

T. Takemura, Research Institute for Applied Mechanics, Kyushu University, 6-1 Kasuga-koen, Kasuga, Fukuoka 816-8580, Japan. (toshi@riam.kyushu-u.ac.jp)